Supporting Online Material: Encircling exceptional points as a non-Hermitian extension of rapid adiabatic passage

J. Feilhauer, A. Schumer, J. Doppler, A. A. Mailybaev,
J. Böhm, U. Kuhl, N. Moiseyev, and S. Rotter

April 7, 2020

Closed semicircular loop in the general two-level model

In order to relate rapid adiabatic passage (RAP) and the chiral state transfer resulting from encircling of an exceptional point (EP) along a closed loop, we prove here that guiding the Hamiltonian of a system along an open semicircular trajectory such that it exhibits RAP is effectively equal to the corresponding closed semicircular loop. Of course, this only holds true if the semicircle is closed along the line defined as $\Omega = 0$ (no coupling).

In the following we only discuss the clockwise (CW) passage of the semicircular loop from the main text which consists of the semicircle $SC_{A\to B}$ and the straight line $L_{B\to A}$. A suitable parametrization for $SC_{A\to B}$ reads

$$\Omega_{\mathrm{SC}}(t) = r\sin(\pi t/T_{\mathrm{SC}}), \tag{S.1}$$

$$\Delta_{\mathrm{SC}}(t) = -r\cos(\pi t/T_{\mathrm{SC}}) + \rho, \tag{S.2}$$

with $0 \le t \le T_{\mathrm{SC}}$. The starting point A and end point B are located at $\Omega = 0$. The linear part $L_{B\to A}$ of the loop is defined as

$$\Omega_{\mathrm{L}}(t) = 0, \tag{S.3}$$

$$\Delta_{\mathrm{L}}(t) = r[1 - 2(t - T_{\mathrm{SC}})/T_{\mathrm{L}}] + \rho, \tag{S.4}$$

with $T_{\mathrm{SC}} < t < T$, where T is the total evolving time along the loop, $T = T_{\mathrm{SC}} + T_L$.

As the time evolution along the straight line $L_{B\to A}$ occurs while the levels are decoupled (i.e. $\Omega_L = 0$), we can write down the analytical solution of the Schrödinger equation

$$c_1(T) = e^{i\int_{T_{\mathrm{SC}}}^{T}\Delta_L(t')dt'/2}\, e^{-\gamma T_{\mathrm{L}}/2}\, c_1(T_{\mathrm{SC}}), \tag{S.5}$$

$$c_2(T) = e^{-i\int_{T_{\mathrm{SC}}}^{T}\Delta_L(t')dt'/2}\, e^{+\gamma T_{\mathrm{L}}/2}\, c_2(T_{\mathrm{SC}}), \tag{S.6}$$

where $c_i(T_{\rm SC})$ and $c_i(T)$, $i = 1, 2$, are the level amplitudes after traversing the semicircle $SC_{A\to B}$ and the semicircular loop ($SC_{A\to B}$, $L_{B\to A}$), respectively. In the Hermitian case, i.e. for $\gamma = 0$, the linear part $L_{B\to A}$ necessary to close the loop only generates a phase factor. To eliminate the influence of the linear part in the general case ($\gamma \neq 0$), we let $T_L \to 0$. As the levels are perfectly decoupled along $L_{B\to A}$ this does not influence the overall adiabaticity of the loop. Then we get $T = T_{\rm SC}$ which is already used in Eqs. (4) and (5) in the definitions of the semicircular loop in the main text. The closing of the loop is therefore fictitious and it only serves the purpose of illustrating the accumulation of the geometric phase of the eigenvectors and the resulting swap with respect to the initial eigenbasis. Equations (S.1–S.4) define a semicircular loop traversed in CW direction. For the corresponding counterclockwise (CCW) encirclement, the first segment of the loop is the linear part $L_{A\to B}$ followed by the semicircle $SC_{B\to A}$. Based on the same reasoning we can neglect the linear part also for the CCW case.

Adiabaticity in the Hermitian case

As RAP relies on the state vector to adiabatically follow an eigenstate when the time evolution is governed by a Hermitian Hamiltonian

$$H_0(t) = \frac{1}{2}\begin{bmatrix} -\Delta(t) & \Omega(t) \\ \Omega(t) & \Delta(t) \end{bmatrix}, \tag{S.7}$$

the parameter cycle should be carried out sufficiently slowly to avoid unwanted non-adiabatic population transfer. Adiabaticity is secured when during the time evolution driven by $H_0(t)$ the state vector $\vec{\psi}(t)$, initially prepared in an eigenstate $\vec{r}_\pm(0)$, remains close to the same instantaneous eigenstate $\vec{r}_\pm(t)$. This condition can be quantified [1] as

$$\tilde{\Omega}(t) = \sqrt{\Omega(t)^2 + \Delta(t)^2} \gg |d\theta(t)/dt|, \tag{S.8}$$

where $\tilde{\Omega}$ represents the energy gap between the upper and lower eigenenergy sheets of Eq. (S.7) for a given Ω and Δ while θ represents the phase angle. Moreover, $\tilde{\Omega}$ also equals the length of the vector (Δ, Ω) [see inset of Fig. S1] oriented at an angle θ that satisfies $\tan\theta = \Omega/\Delta$. Therefore, the graphical interpretation of the adiabaticity condition in Eq. (S.8) states that during the adiabatic passage the length of the vector $\vec{\tilde{\Omega}}$ should be much larger than its angular velocity. For the semicircular part of the loop, the passage time T and the radius r can be tuned to satisfy the condition while for the linear part θ is constant and the evolution therefore perfectly adiabatic. The values of Eq. (S.8) for the loop in Fig. 2(a) in the main text are shown in Fig. S1. Obviously, the adiabaticity condition is perfectly satisfied throughout the entire passage along the semicircular loop.

We can also test the adiabaticity condition for wave transport in the finite bimodal waveguide without absorber when considering the Hermitian part of

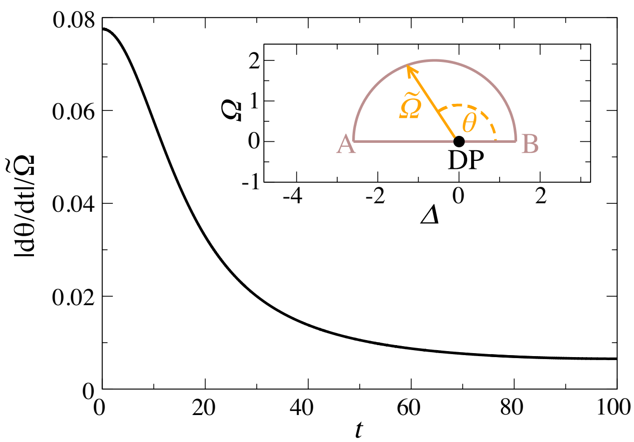

Figure S1: Tracking the adiabaticity condition $|d\theta/dt|/\tilde{\Omega} \ll 1$ when traversing the semicircular parameter loop displayed in Fig. 1(a) in the main text (see also inset). Clearly, the condition is perfectly satisfied in the simplified Hermitian model.

the Hamiltonian [see Eq. (S.64)]. The obtained values of $|d\theta/dt|/\tilde{\Omega}$ shown in Fig. S2 confirm that the adiabaticity condition is satisfied also for the simulation of the microwave waveguide.

Dynamical evolution: Hermitian versus non-Hermitian system

In this section we analyze the dynamic evolution of the symmetric switch inherent in RAP and the asymmetric state transfer connected to encircling of an EP. We assume the general Hamiltonian

$$\mathcal{H} = \frac{1}{2}\begin{bmatrix} -\Delta - i\gamma & \Omega \\ \Omega & \Delta + i\gamma \end{bmatrix}, \tag{S.9}$$

with complex eigenvalues $\lambda_\pm = \pm\lambda$, where $\lambda = \sqrt{(\Delta + i\gamma)^2 + \Omega^2}/2$, and right eigenstates $\mathcal{H}\vec{r}_\pm = \lambda_\pm \vec{r}_\pm$ defined as

$$\vec{r}_- = \begin{pmatrix} \cos\vartheta/2 \\ \sin\vartheta/2 \end{pmatrix}, \quad \vec{r}_+ = \begin{pmatrix} -\sin\vartheta/2 \\ \cos\vartheta/2 \end{pmatrix}, \tag{S.10}$$

where ϑ satisfies $\tan\vartheta = -\Omega/(\Delta + i\gamma)$. Then the solution of the Schrödinger equation $i\partial\vec{\psi}(t)/\partial t = \mathcal{H}(t)\vec{\psi}(t)$ can be expanded in the basis of the instantaneous eigenvectors in the form

$$\vec{\psi}(t) = c_-(t)\vec{r}_-(t) + c_+(t)\vec{r}_+(t), \tag{S.11}$$

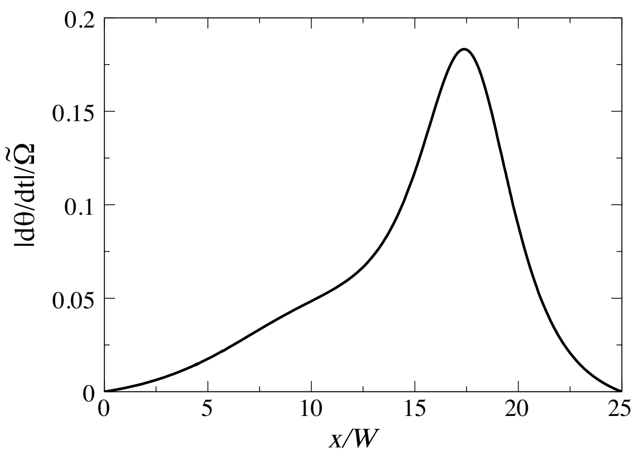

Figure S2: Tracking the adiabaticity condition $|d\theta/dt|/\tilde{\Omega} \ll 1$ when passing the lossless waveguide according to the parametric loop shown in Fig. 3(a) of the main text. The condition is again satisfied.

where $c_\pm(t)$ are the complex amplitudes of the state vector in the instantaneous eigenbasis.

To visualise the dynamical evolution along the semicircular loop in the Hermitian and non-Hermitian system we project the evolving state onto the real part of the eigenspectrum. The corresponding trajectories with the vertical coordinate defined as

$$\frac{\mathrm{Re}\left[\lambda_+(t)\right]|c_+(t)|^2 + \mathrm{Re}\left[\lambda_-(t)\right]|c_-(t)|^2}{|c_+(t)|^2 + |c_-(t)|^2} \tag{S.12}$$

are shown in Fig. S3. The left column shows the dynamic evolution in the Hermitian system ($\gamma = 0$) along the closed semicircular loop crossing the diabolic point (DP). In CW as well as in CCW direction the eigenstates interchange symmetrically confirming successful RAP. The right column then shows the evolution in the non-Hermitian system along the same semicircular parametric loop which now encircles the EP. As a result of the occurring sudden non-adiabatic jumps between the loss (blue) and gain (red) parts of the eigenspectra, the final states at the end of the loop depend only on the encircling direction and are independent of the initial state confirming the chiral state transfer (i.e. asymmetric switching).

Crossover between symmetric and asymmetric switching

In the previous section we have shown that adding a suitable amount of loss to RAP schemes can turn the symmetric state transfer into an asymmetric one.

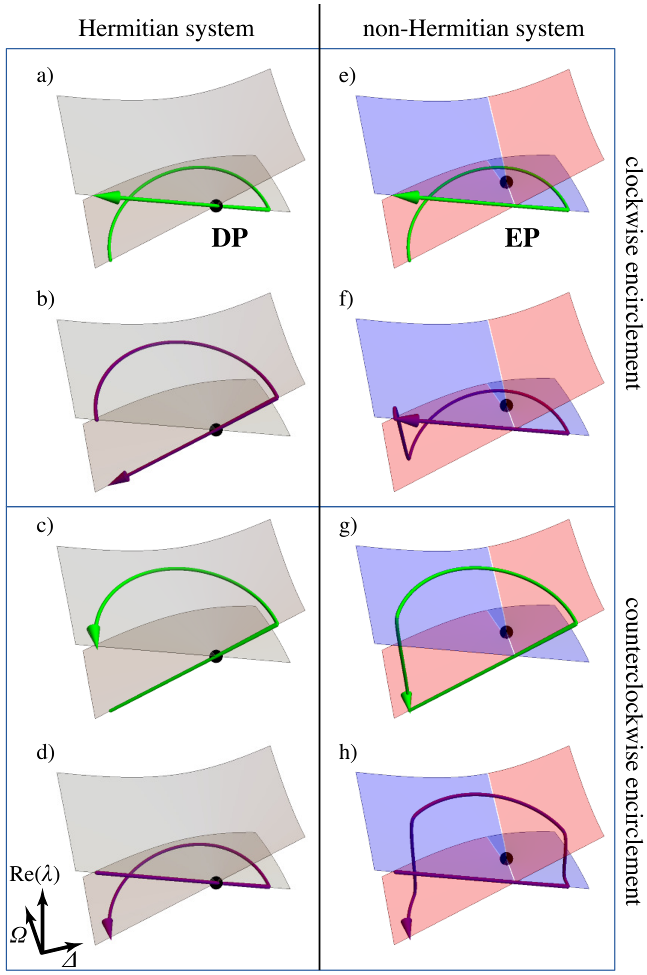

Figure S3: Clockwise (top panels) and counterclockwise (bottom panels) passage along a semicircular loop crossing the DP (left panels) and encircling the EP (right panels). The arrows show a projection of the evolving state onto the real part of the eigenspectrum according to Eq. (S.12). Violet and green arrows show the state evolution starting at the first and second level, respectively. Red (gain) and blue (loss) regions represent the eigenvalues with $\mathrm{Im}\lambda_{\pm} > 0$ and $\mathrm{Im}\lambda_{\pm} < 0$, respectively.

The goal in this section is to determine the critical loss contrast γ_c that has to be added to a semicircular loop such that the system then exhibits an asymmetric switching. As it turns out, for finite loop times T there are in fact two boundaries (γ_c^{off} and γ_c^{on}) that converge towards γ_c [Eq. (6) in the main text] in the limit $T \to \infty$ [see Fig. S4]: the two encircling directions independently switch their behavior, such that at first an additional non-adiabatic jump in one direction turns off the symmetric state transfer at γ_c^{off}. When the loss contrast is increased further to $\gamma_c^{\mathrm{on}} \geq \gamma_c^{\mathrm{off}}$, the non-adiabatic jump in the other encircling direction is suddenly inhibited and the overall state transfer becomes asymmetric.

Before we calculate the boundary between the symmetric and asymmetric region, we want to define a measure that allows to quantify the faithfulness of the symmetric and asymmetric state transfer and that highlights the boundaries between those two regimes. For this purpose we firstly combine the values of level population p [Eq. (5) in the main text] at the beginning and end of the evolution as

$$S_j = p_j(t=0)p_j(t=T), \quad j = 1, 2\,, \tag{S.13}$$

which equals -1 if the eigenstate at the end does not resemble the initial one or $+1$ if the state vector returns back to the initial level. Then considering the state switching in the CW and CCW encircling direction we can define the switching parameter

$$\alpha = \frac{S_1^{\mathrm{CW}} S_2^{\mathrm{CW}} + S_1^{\mathrm{CCW}} S_2^{\mathrm{CCW}} + S_1^{\mathrm{CW}} S_1^{\mathrm{CCW}} + S_2^{\mathrm{CW}} S_2^{\mathrm{CCW}}}{4}. \tag{S.14}$$

The value -1 represents asymmetric switching (chiral state transfer) and $+1$ characterizes symmetric switching. The breakdown of the symmetric region occurs when $0 \leq \alpha \lesssim 1/2$ and the onset of the asymmetric regions occurs if $0 \geq \alpha \gtrsim -1/2$. The particular definition of α allows to distinguish between the breakdown of the symmetric region and the onset of the asymmetric state transfer. When the system is transitioning from a symmetric to an asymmetric state transfer then $\alpha \approx 0$. However, when the loss contrast γ becomes too large, the state vector simply ends up in the eigenstate that is subject to gain at the end of the loop for any initial configuration and $\alpha = 0$. The map of the switching parameter α is shown in Fig. 2(e) in the main text as a function of the loop's offset ρ and loss/gain strength γ.

As can be recognized in Figs. 2(c) and 2(d) in the main text, the collapse of symmetric switching is related to the asymmetry of the CW and CCW evolution of the state initially populating the gain eigenvector (green curves). At the early part of the evolution this eigenstate is amplified and the evolution is adiabatic until the loop crosses the $\mathrm{Im}\,\lambda = 0$ line at the critical time t_* (dashed vertical line), which is different for each encircling direction due to the loop's offset ρ. For $t > t_*$ the same eigenstate is suddenly attenuated and the adiabatic evolution becomes unstable. The onset of a non-adiabatic jump from the now attenuated towards the instantaneously amplified eigenstate, however, occurs at a delayed time $t = t_+ > t_*$ [3]. For $\rho < 0$ the critical time t_* in the CW direction is larger than $T/2$ and hence $t_+ > T$, which inhibits a non-adiabatic jump for a single passage of the loop. However, for CCW encirclement we have $t_* < T/2$ and for a sufficiently large asymmetry $|\rho|$ we get $t_+ < T$, i.e. a non-adiabatic transition occurs, which marks the breakdown of the symmetric state transfer.

To derive an analytical formula for the border between the regions of symmetric and asymmetric switching we utilize the formalism of stability loss delay described in detail in [3]. In accord with the expansion in Eq. (S.11) we start by introducing the time evolution operator $\mathcal{U}$ defined via $\vec{\psi}(t) = \mathcal{U}(t)\vec{\psi}(0)$ with

$$\dot{\mathcal{U}} = -i \begin{bmatrix} -\lambda(t) & -f(t) \\ f(t) & \lambda(t) \end{bmatrix} \mathcal{U}, \quad \mathcal{U} = \begin{bmatrix} U_{-,-} & U_{-,+} \\ U_{+,-} & U_{+,+} \end{bmatrix}, \tag{S.15}$$

where

$$f(t) = \frac{\Omega(t)\dot{\Delta}(t) - (\Delta(t) + i\gamma)\dot{\Omega}(t)}{8i\lambda^2(t)} \tag{S.16}$$

is the non-adiabatic coupling of the eigenstates. Then we define the non-adiabatic transition amplitude

$$R(t) = \frac{U_{-,+}(t)}{U_{+,+}(t)}, \tag{S.17}$$

which resembles adiabaticity of the dynamic evolution starting from the state populating solely the eigenvector $\vec{r}_+$. If $|R| \ll 1$ the state is evolving adiabatically while for $|R| \gg 1$ a non-adiabatic jump has occurred during the evolution. The non-adiabatic transition amplitude $R(t)$ is a solution of the nonlinear differential equation

$$\dot{R}(t) = 2i\lambda(t)R(t) + if(t)\left[1 + R(t)^2\right], \tag{S.18}$$

with the initial condition $R(0) = 0$. The solution to Eq. (S.18) follows one of two fixed points with fast non-adiabatic transitions between them. The fixed points are well approximated by

$$R^{\mathrm{ad}}(t) \simeq -\frac{f(t)}{2\lambda(t)}, \quad R^{\mathrm{nad}}(t) \simeq -\frac{2\lambda(t)}{f(t)}, \tag{S.19}$$

with $\left|R^{\mathrm{ad}}(t)\right| \ll 1$, $\left|R^{\mathrm{nad}}(t)\right| \gg 1$ and $R^{\mathrm{ad}}(t)R^{\mathrm{nad}}(t) = 1$. Therefore, the time t_+ corresponding to the position of a non-adiabatic jump can be determined by the condition

$$|R(t_+)| = 1. \tag{S.20}$$

As long as the loss contrast γ is sufficiently small the solution $R(t)$ to Eq. (S.18) will simply follow $R^{\mathrm{ad}}(t)$. Upon the increase of γ a non-adiabatic transition will set in, which demarcates the breakdown of the symmetric switching behavior. To pinpoint the exact location of this boundary we define the critical loss contrast γ_c such that the non-adiabatic transition happens exactly at the end of the parameter path, i.e.

$$|R(t_+ = T)| = 1. \tag{S.21}$$

At first, we require a suitable approximation for $R(t)$ that correctly reproduces the position of the non-adiabatic jump. We consider initially a stable adiabatic evolution where $R(t)$ closely follows $R^{\mathrm{ad}}(t)$. Then Eq. (S.18) can be linearized

$$\dot{R}(t) = 2i\lambda(t)R(t) + if(t) \tag{S.22}$$

with the solution

$$R(t) = R(0)e^{\Phi(t)} + i\int_0^t f(t')e^{\Phi(t)-\Phi(t')}dt', \tag{S.23}$$

where

$$\Phi(t) = 2i\int_0^t \lambda(t')dt'. \tag{S.24}$$

Expanding the integral in Eq. (S.23) through an N-times integration by parts and utilizing the properties of asymptotic series we can rewrite the non-adiabatic transition amplitude in the form

$$R(t) \simeq \mathcal{R}^{\rm ad}(t) + D(t)e^{\Phi(t)-\Phi(t_*)} + Ae^{\Phi(t)}, \tag{S.25}$$

where

$$\mathcal{R}^{\rm ad}(t) = \sum_{n=0}^{N-1}\left(\frac{1}{2i\lambda(t)}\frac{d}{dt}\right)^n R^{\rm ad}(t) \tag{S.26}$$

is an optimally truncated correction to $R^{\rm ad}(t)$, $D(t)$ is the remaining part of the solution not included in the sum in Eq. (S.26) and

$$A = R(0) - \mathcal{R}^{\rm ad}(0) \tag{S.27}$$

reflects how the value of R initially differs from the adiabatic fixed point $R^{\rm ad}$. The second and third term in Eq. (S.25) are attenuated until $t = t_*$ therefore for $t < t_*$ the adiabatic term $\mathcal{R}^{\rm ad}(t)$ dominates. For $t > t_*$, the second and third term in Eq. (S.25) start to grow exponentially and in the vicinity of t_+ they outgrow the adiabatic term, which leads to the onset of the non-adiabatic transition. To examine the condition Eq. (S.20) we are interested in R in the vicinity of t_+. Therefore, we can neglect the adiabatic term $\mathcal{R}^{\rm ad}(t)$ in Eq. (S.25). Moreover, as discussed in [3], in the case of a single passage of the loop the non-adiabatic transition is driven by the third term in Eq. (S.25) since the solution R does not have enough time to approach the adiabatic fixed point $R^{\rm ad}$ sufficiently closely by the critical time t_*. Then we can approximate R in the vicinity of t_+ as

$$R(t_+) \simeq Ae^{\Phi(t_+)}. \tag{S.28}$$

Since $R(0) = 0$ and the sum in Eq. (S.26) is well approximated at $t = 0$ by its 0-th term we can write

$$A = -\mathcal{R}^{\rm ad}(0) \approx -R^{\rm ad}(0) \simeq \frac{f(0)}{2\lambda(0)}. \tag{S.29}$$

This gives us a viable approximation for R in the vicinity of the non-adiabatic transition

$$R(t_+) \simeq \frac{f(0)}{2\lambda(0)}e^{\Phi(t_+)}. \tag{S.30}$$

To identify the critical loss contrast γ_c defining the border between the regions of symmetric and asymmetric evolution, we continue by inserting Eq. (S.30) into the boundary condition [Eq. (S.21)]

$$\left| \frac{f(0)}{2\lambda(0)} e^{\Phi(T)} \right| = \left| \frac{f(0)}{2\lambda(0)} \right| e^{\mathrm{Re}[\Phi(T)]} = 1. \tag{S.31}$$

Employing the definition of the semicircular loop [Eqs. (3) and (4) in the main text] we obtain the eigenvalues λ in the form

$$\begin{aligned} \lambda(t) &= \frac{r}{2}\sqrt{1+\Gamma^2+2\Gamma\cos(\pi t/T)} \\ &= \frac{r}{2}\left\{1+\Gamma\cos\left(\frac{\pi t}{T}\right)+\frac{\Gamma^2}{2}\left[1-\cos^2\left(\frac{\pi t}{T}\right)\right]\right\}+\mathcal{O}(\Gamma^3), \end{aligned} \tag{S.32}$$

with $\Gamma = (\rho + i\gamma)/r$, where we expanded λ around $\Gamma = 0$. Then

$$\Phi(T) = 2i\int_0^T \lambda(t')dt' \approx irT\left(1+\frac{\Gamma^2}{4}\right), \tag{S.33}$$

which yields

$$\mathrm{Re}[\Phi(T)] \approx -\frac{\rho\gamma T}{2r}. \tag{S.34}$$

Using Eqs. (S.16) and (S.32) we get

$$\left|\frac{f(0)}{2\lambda(0)}\right| = \left|\frac{i\pi}{2Tr}\frac{1}{(1+\Gamma)^2}\right| = \frac{\pi}{2Tr}\frac{1}{(\gamma/r)^2+(1+\rho/r)^2}. \tag{S.35}$$

Finally, we can rewrite the condition from Eq. (S.31) into the form

$$\frac{\pi}{2Tr}\frac{e^{-\frac{\rho\gamma T}{2r}}}{(\gamma/r)^2+(1+\rho/r)^2} = 1. \tag{S.36}$$

Assuming $\gamma \ll r + \rho$ we can obtain the border for the breakdown of the symmetric state transfer in an analytical form

$$\gamma_c^{\mathrm{off}} \simeq \frac{2r}{T\rho}\ln\left[\frac{\pi r}{2T(\rho+r)^2}\right]. \tag{S.37}$$

In the derivation of Eq. (S.37) we assumed $\rho < 0$. When $\rho > 0$ the non-adiabatic transition that determines the end of the symmetric switch occurs in the opposite encircling direction. The procedure for the approximation of the critical loss rate is analogous though and so the formula that is valid for all values of ρ is

$$\gamma_c^{\mathrm{off}} \simeq \frac{2r}{T|\rho|}\ln\left[\frac{2T(r-|\rho|)^2}{\pi r}\right]. \tag{S.38}$$

As mentioned before, this particular loss contrast solely determines the point at which the system does not show a symmetric switch in both directions anymore.

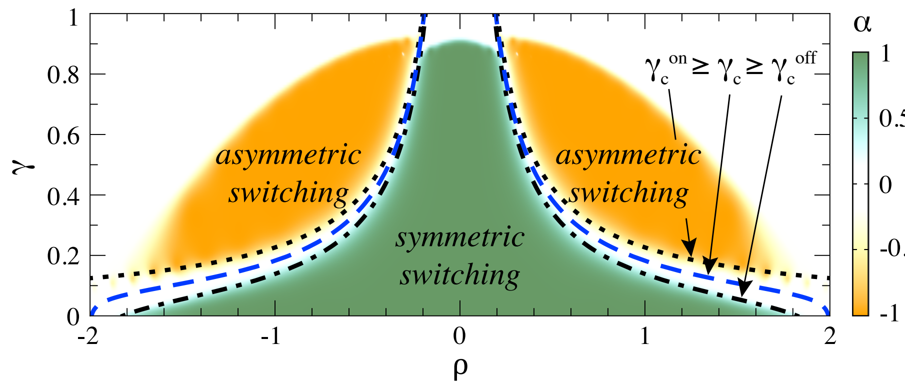

Figure S4: The same map as in the main text depicting the state switch asymmetry when numerically following $SC_{A\to B}$ in both encircling directions as a function of the loop offset ρ and the loss-gain value γ. The shown switching parameter α takes on its limiting values 1 (-1) for a symmetric (asymmetric) switch as in RAP (as in the chiral state transfer). The two boundaries $\gamma_c^{\rm off}$ (black dot-dashed line) and $\gamma_c^{\rm on}$ (black dotted line) demarcate the breakdown of the symmetric state transfer and the onset of the asymmetric switching behavior, respectively. In the limit of quasi-adiabatic passage, i.e. $T\to\infty$, those boundaries converge towards γ_c shown as a blue dashed line.

However, the encircling direction in which the $\mathrm{Im}\,\lambda = 0$ line is crossed later in time still shows the symmetric state transfer although the final state can have a considerable non-adiabatic contribution.

In this regard, Eq. (S.38) solely specifies the onset of a non-adiabatic transition in one direction. The derivation in the opposite direction follows the same procedure and the critical loss contrast for the onset of the asymmetric switching behavior can be obtained by simply setting $r\to -r$ and $T\to -T$, which reverses the parameter path. The critical loss turns out to be

$$\gamma_c^{\rm on} \simeq \frac{2r}{T|\rho|}\ln\left[\frac{2T(r+|\rho|)^2}{\pi r}\right]. \tag{S.39}$$

It holds that $\gamma_c^{\rm on} \geq \gamma_c^{\rm off}$ where the equality only hold in the limit $T\to\infty$. The value at which both of them converge when the loop time T is increased is their mean value

$$\gamma_c \simeq \frac{2r}{T|\rho|}\ln\left[\frac{2T(r^2-\rho^2)}{\pi r}\right], \tag{S.40}$$

shown as a blue dashed line in Fig. 2(e) in the main text. In Fig. S4 those three boundaries $\gamma_c^{\rm on} \geq \gamma_c \geq \gamma_c^{\rm off}$ are drawn on the same map of the switching parameter as in Fig. 2(e) in the main text.

Hamiltonian of the waveguide with absorber

The procedure of how to convey the temporal evolution of a quantum state driven by a 2×2-Hamiltonian to the spatial distribution of microwaves along a bimodal waveguide was described and derived in detail in [2]. First, we briefly summarize the main ideas of this process. Then, in addition to the results presented in [2], we apply the model to the waveguide with the continuous position-dependent absorber in order to support the numerical results of microwave transport with the calculations based on the semi-analytical model.

In the two-dimensional waveguide, the propagation of microwaves with frequency ω can be described by the state $\varphi(x,y,t)=\phi(x,y)e^{-i\omega t}$ satisfying the Helmholtz equation

$$\Delta\phi(x,y)+\epsilon(x,y)k^2\phi(x,y)=0, \tag{S.41}$$

where $k=\omega/c$ and $\epsilon(x,y)=1+i\eta(x,y)/k$ is a complex dielectric function with $\eta(x,y)$ describing the losses to the environment and to an absorber located in the waveguide interior.

We study wave transmission through a 2D waveguide with constant (transverse) width W and periodically modulated edges described by a profile $\xi(x)=\sigma\sin(k_b x)$. Hard wall boundary conditions are assumed at $y=\xi(x)$ and $y=W+\xi(x)$.

The microwave wavefunction in this periodic waveguide can be described through a Bloch wave ansatz

$$\phi(x,y)=\Lambda(x,y)e^{iKx}, \tag{S.42}$$

where K is a wave number reduced to the first Brillouin zone and $\Lambda(x,y)=\Lambda(x+l,y)$ is a periodic function with the period of the edge modulation $l=2\pi/k_b$. In the case of a straight waveguide ($\sigma=0$) without losses ($\eta=0$), $\Lambda(x,y)$ has a simple form

$$\Lambda^0_{mn}(x,y)=e^{ik_b mx}\sin\left(\frac{\pi ny}{W}\right), \tag{S.43}$$

and the corresponding wave number $K^0\in[-k_b/2,k_b/2]$ is given by

$$k^2=\left(k_b m+K^0\right)^2+\left(\frac{\pi n}{W}\right)^2. \tag{S.44}$$

Tuning the waveguide width W and/or the frequency ω of the microwaves such that $2\pi/W<k<3\pi/W$, we reduce the number of propagating modes to two, i.e. $n=1,2$.

It is known in wave scattering theory for waveguides with modulated boundaries that when the boundary oscillations are given by $k_b=k_r=k_1-k_2$, where $k_j=\sqrt{k^2-(\pi j/W)^2}$, both propagating modes experience resonant forward scattering and backscattering of microwaves is negligible. Therefore, we can assume that when k_b is close to k_r, i.e. $k_b=k_r+\delta$, where δ denotes a shift from the forward scattering resonance, the wave is moving only in one direction (e.g. from left to right or vice versa) and K has the same sign for all possible solutions [Eq. (S.42)]. Then for a given ω there are two right-propagating solutions of Eq. (S.41) in the straight waveguide given by

$$\phi_j(x,y) = e^{iK_j^0 x}\Lambda_j^0(x,y), \quad \Lambda_j^0(x,y) = e^{ik_b m_j x}\sin\left(\frac{\pi j y}{W}\right), \tag{S.45}$$

where $j=1,2$, $K_j^0>0$ and m_j are given by Eq. (S.44). Setting $k_b = k_r = k_1 - k_2$ (i.e. $\delta = 0$) we get $m_2 = m_1 - 1$ and $K_1^0 = K_2^0 = K^0$, which means that the states from Eq. (S.45) are degenerate with respect to the Bloch wave number K. In the following, we will study how this degeneracy is lifted when introducing a finite (but small) periodic modulation of the waveguide edges parametrized by the amplitude σ and shift δ.

Treating the edge modulations as a small perturbation we can write the perturbed Bloch solution of Eq. (S.41) in the form

$$\phi(x,y) \approx \left(a_1\Lambda_1^0(x,y) + a_2\Lambda_2^0(x,y)\right)e^{i(K^0+s)x}, \tag{S.46}$$

where s is a small correction to the Bloch wave number. Following [2], utilizing a perturbative approach by keeping only the first-order terms in σ, δ, η and s, the Helmholtz equation (S.41) can be rewritten into a pair of algebraic equations for the coefficients a_1 and a_2. Then, using the substitution

$$c_1(x) = i\sqrt{k_1}e^{-i(\delta/2-s)x}a_1, \tag{S.47}$$

$$c_2(x) = -i\sqrt{k_2}e^{-i(\delta/2-s)x}a_2, \tag{S.48}$$

these algebraic equations can be recast into a Schrödinger-like equation

$$i\frac{\partial}{\partial x}\begin{pmatrix}c_1\\c_2\end{pmatrix} = H\begin{pmatrix}c_1\\c_2\end{pmatrix}, \tag{S.49}$$

where the Hamiltonian describing the microwave transport in the bimodal waveguide with periodically modulated edges can be written as

$$H = \frac{1}{2}\begin{bmatrix}\delta & 2B\sigma\\ 2B\sigma & -\delta\end{bmatrix} - i\frac{\eta_0 k}{2}\begin{bmatrix}\Gamma_{11} & \Gamma_{12}\\ \Gamma_{12}^* & \Gamma_{22}\end{bmatrix}, \tag{S.50}$$

where $B = 2\pi^2/W^3\sqrt{k_1k_2}$ and

$$\Gamma_{nm} = \frac{e^{i\pi(m-n)/2}}{\sqrt{k_nk_m}}\frac{2}{Wl} \times \int_0^l\int_0^W \tilde{\eta}(x,y)\sin\left(\frac{n\pi}{W}y\right)\sin\left(\frac{m\pi}{W}y\right)e^{-i(k_n-k_m)x}dx\,dy \tag{S.51}$$

with $\tilde{\eta}(x,y) = \tilde{\eta}(x+l,y)$ specifying the periodic spatial distribution of the absorber in the waveguide. In the case of homogeneous bulk absorption [$\tilde{\eta}(x,y) =$

1] the Hamiltonian takes a simple form

$$H_{\mathrm{hom}} = \frac{1}{2}\begin{bmatrix} \delta & 2B\sigma \\ 2B\sigma & -\delta \end{bmatrix} - i\frac{\eta_0 k}{2}\begin{bmatrix} \frac{1}{k_1} & 0 \\ 0 & \frac{1}{k_2} \end{bmatrix}. \tag{S.52}$$

Using the proper substitution outlined in [3], the Hamiltonian describing homogeneous bulk absorption in the waveguide [Eq. (S.52)] is directly comparable with the model Hamiltonian for a two-level system with gain and loss [Eq.(1) in the main text], which we used to demonstrate the connection between RAP and the chiral state transfer. However, as was shown in [2], a homogeneous absorption drastically attenuates the microwaves inside the waveguide, which makes such a system impractical for experimental realization.

To overcome this issue and to additionally optimize the performance of the asymmetric switching device the loss contrast between the eigenmodes of the Hamiltonian in Eq. (S.50) has to be maximized. It was proposed in [2] that the optimal position of the absorber is located at the nodes of one eigenmode. Then, this eigenmode is almost unaffected by damping while, on the other hand, the second eigenmode is strongly attenuated since the absorber is placed in the vicinity of its maxima. However, since those nodes are discrete points concentrating the absorption only in the nodes would cause significant backscattering of microwaves. Therefore, in the semi-analytical model from [2] the absorption smoothly changes in the vicinity of the nodes modelled by Gaussian peaks with a finite width sufficient enough to minimize backscattering.

Due to mechanical and material limitations of realistic absorbers it is very challenging to realize the above concept experimentally. Moreover, it would be necessary to locate the nodes with very high precision which by itself is a very difficult task. Therefore, in the numerical and experimental setup in [2], the authors used a continuous thin absorber that was placed such that it interpolates between the nodes. This leads to some parasitic damping of the eigenmode that one wanted to keep free of attenuation, but it did otherwise not affect the results studied there.

The numerical and experimental results of microwave transport in a waveguide with a continuous position-dependent absorber [2] confirm the successful asymmetric switching. What has been missing so far, however, is a semi-analytical model based on the Schrödinger equation (S.49) describing the transmission through such a waveguide. In the next subsections we introduce the Hamiltonian for a waveguide with a continuous position-dependent absorber and compare the spatial evolution of microwaves driven by this Hamiltonian with the numerical simulation of the microwave transport based on the method of recursive Green's functions.

Potential of the continuous position-dependent absorber

As discussed above, the position of the thin continuous absorber is taken from an interpolation between the nodes of one eigenfunction of the Hermitian (lossless) part of the Hamiltonian in Eq. (S.50), i.e.

$$H_0 = \frac{1}{2}\begin{bmatrix} \delta & 2B\sigma \\ 2B\sigma & -\delta \end{bmatrix}. \tag{S.53}$$

The corresponding Bloch eigenfunctions are given by Eq. (S.46) with coefficients a_1 and a_2 related to the eigenvectors of Eq. (S.53) via Eq. (S.47). This yields

$$a_2 = -i\sqrt{\frac{k_1}{k_2}}\frac{\delta + (-1)^j\sqrt{\delta^2 + 4B^2\sigma^2}}{2B\sigma}a_1, \quad j = 1, 2 \tag{S.54}$$

for the j-th eigenvector of (S.53). Then, there are two nodes of the Bloch eigenfunctions located in the unit cell of the periodic waveguide which are periodically distributed along the waveguide at

$$x_o = \pm l/4 + lo, \quad o \in \mathbb{Z} \tag{S.55}$$

$$y_o = \frac{W}{\pi}\arccos\left(\pm(-1)^j\frac{|a_1|}{2\,|a_2|}\right). \tag{S.56}$$

As will be clear later we are interested in the node positions of the eigenfunction which is for $\delta < 0$ and negligible amplitude of the edge oscillations σ almost entirely equal to $\Lambda_2^0(x, y)$. Therefore, in the next text we assume $j = 2$. To interpolate between the nodes we use a sine function of the form

$$y_{int} = \frac{W}{2} + u\sin\left(\frac{2\pi x}{l}\right), \tag{S.57}$$

centered along the longitudinal axis of the waveguide with amplitude

$$u = \frac{W}{\pi}\arccos\left(\frac{|a_1|}{2\,|a_2|}\right) - \frac{W}{2}. \tag{S.58}$$

In the case of a straight waveguide ($\sigma = 0$) one of the eigenfunctions is given by $\phi_2(x, y)$, which means $a_1 = 0$. In this case, the amplitude u is zero and the absorber is simply placed parallel to the center longitudinal axis of the waveguide, which corresponds to the node of the second propagating eigenstate. An example of a waveguide with nonzero σ is depicted in the lower panel of Fig. S5. The lower panel shows the wave density $|\phi(x, y)|^2$ for $kW/\pi = 2.6$ in an infinite periodic waveguide with boundary parameters $\sigma/W = 0.13$ and $\delta W = 0.15$. The red curve marks the position of the periodic absorber given by Eq. (S.57) interpolating between the nodes of the depicted eigenfunction of Eq. (S.53). Then, the potential of the thin continuous absorber with width d is defined as

$$\tilde{\eta}(x, y) = \Theta\left[y - \frac{W}{2} - u\sin\left(\frac{2\pi x}{l}\right) + \frac{d}{2}\right] + \Theta\left[\frac{W}{2} + u\sin\left(\frac{2\pi x}{l}\right) + \frac{d}{2} - y\right], \tag{S.59}$$

where Θ is the Heaviside step function. Inserting Eq. (S.59) into Eq. (S.51) results in a Hamiltonian [Eq. (S.50)] for the modulated waveguide with the position-dependent continuous absorber.

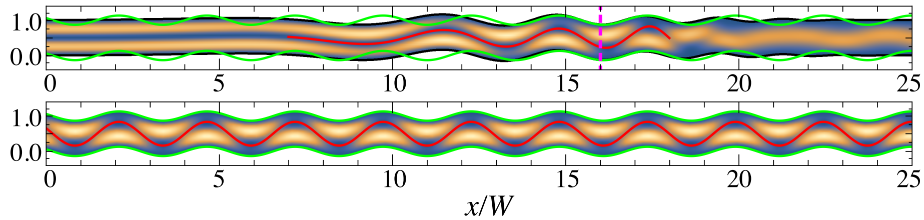

Figure S5: Top: Wave density $|\phi(x,y)|^2$ for $kW/\pi = 2.6$ in the finite waveguide without losses calculated semi-analytically using the Hermitian Hamiltonian Eq. (S.53). The red curve represents the position of the absorber interpolated between the nodes of the wave density. Bottom: Wave density in the infinite periodic waveguide with $\sigma/W = 0.13$ and $\delta W = 0.15$ corresponding to the finite waveguide (top panel) at $x_0 = 16W$ (magenta dashed line). Again, the red curve represents the position of the absorber in the infinite waveguide.

Finite waveguide with position-dependent edge modulation

We have shown that the unidirectional microwave transport in the periodic bimodal waveguide with modulated edges can be mapped onto the evolution of a quantum state, comprised of the complex amplitudes of the microwaves, that evolve according to the Schrödinger equation (S.49) with fixed edge modulation amplitude σ and period δ as well as absorption strength η. Since we are interested in the dynamical evolution of the state driven by a Hamiltonian with analogous time-dependent parameters, we define the microwave system such that the parameters in the Hamiltonian vary along the longitudinal coordinate x. Such a system is realized as a waveguide with finite length $L \gg l$ where the parameters $\sigma(x)$, $\delta(x)$ and $\eta(x)$ vary negligibly slowly on the scale of the edge modulation period l. Then, the microwave transport in such a finite waveguide can be well described by the Schrödinger equation (S.49) with position-dependent parameters. As discussed in the main text, in order to achieve faithful RAP as well as an asymmetric state flip, the variation of the parameters in the Hamiltonian should correspond to a (closed) path which crosses the DP (in the Hermitian case) and encircles an EP (in the non-Hermitian case). The modes at the beginning and end of the evolution are uncoupled which translates to $\sigma = 0$ at both ends of the waveguide. We choose

$$\sigma(x) = \sigma_0 \left[1 - \cos(2\pi x/L)\right] \tag{S.60}$$

to smoothly increase and decrease the amplitude in order to reduce backscattering of microwaves at both waveguide ends. We define the detuning as a linear function of x in the form

$$\delta(x) = \pm\delta_0(2x/L - 1) + \rho, \tag{S.61}$$

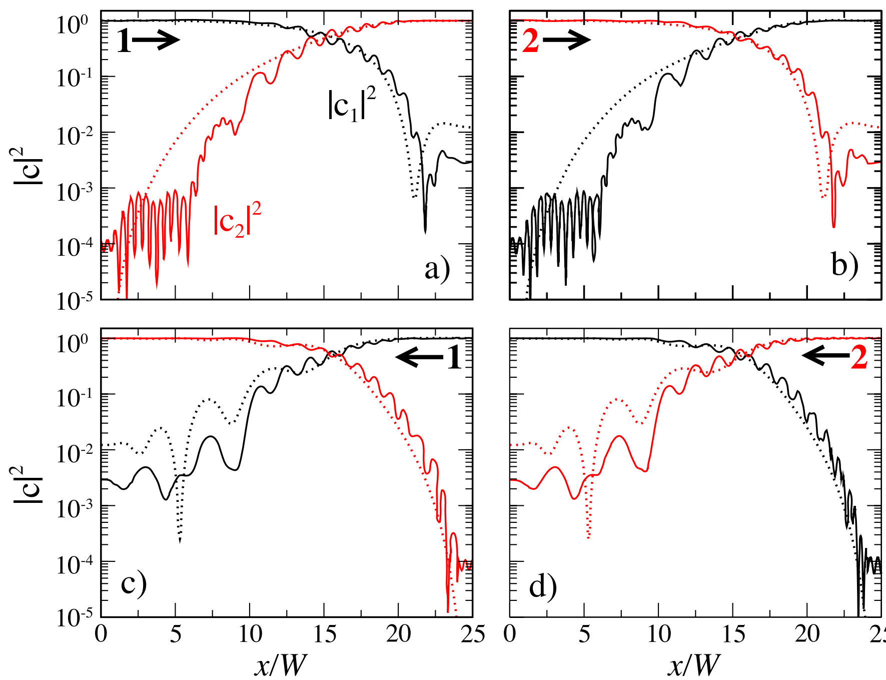

Figure S6: Numerical (solid curves) and semi-analytical (dotted curves) calculation of the modal intensities $|c_1|^2$ (black) and $|c_2|^2$ (red) evolving along the waveguide without absorber. Graphs a) and c) depict the wave entering the waveguide in the first mode from the left and right, respectively. Graphs b) and d) show the same for the wave initially in the second mode. All graphs confirm the successful flip of the mode populations characteristic for RAP.

where the sign corresponds to traversing the loop in CW or CCW direction, respectively. The waveguide with parameters $\sigma_0/W = 0.16$, $\delta_0 W = 1.25$, $\rho W = -1.8$ and $L/W = 25$ used in our numerical simulations and in the experiment is depicted in the top panel of Fig. S5.

However, in the finite waveguide with varying edge modulations the value of the detuning $\delta(x_0)$ at an arbitrary $x = x_0$ is not exactly the parameter that enters the Hamiltonian in Eq. (S.50), as it was derived for an infinite waveguide with periodic edge modulations. As described in [2], to obtain the correct value of detuning, the phase $\alpha(x) = [k_r + \delta(x)]x$ of the boundary $\sigma \sin[\alpha(x)]$ defining the edge of the finite waveguide has to be linearized, i.e. the edge of the infinite waveguide corresponding to $x = x_0$ is defined as $\sigma \sin[\beta(x)]$ where

$$\beta(x) = \left(\left. \frac{d\alpha}{dx} \right|_{x=x_0} \right) x = [k_r + \Delta(x_0)]\, x \tag{S.62}$$

and the renormalized position-dependent detuning entering the Hamiltonian of

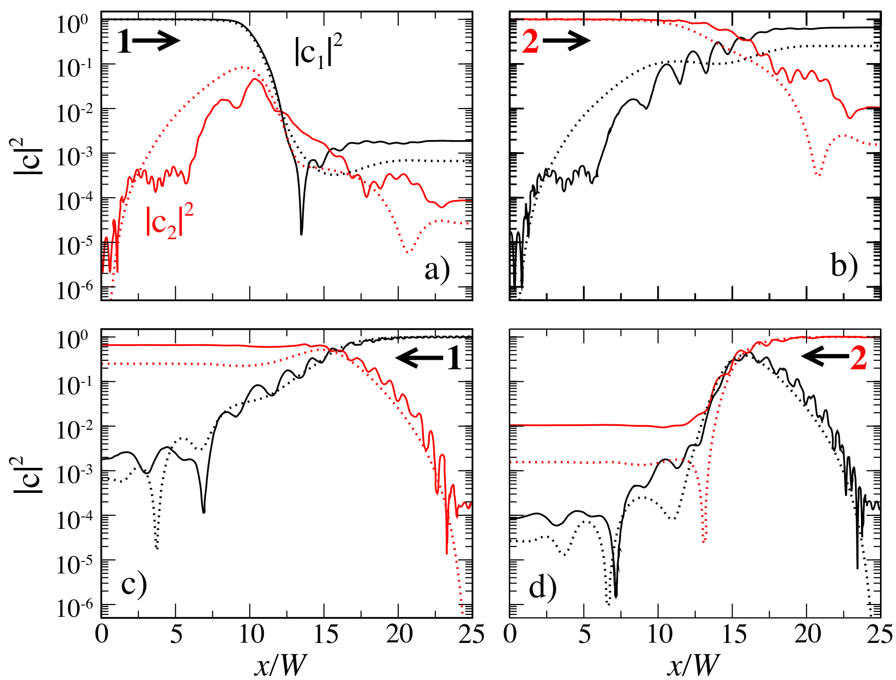

Figure S7: Numerical (solid curves) and semi-analytical (dotted curves) calculation of modal intensities $|c_1|^2$ (black curves) and $|c_2|^2$ (red curves) evolving along the waveguide with position-dependent continuous absorber. Graphs a) and c) depict the wave entering the waveguide in the first mode from the left and right respectively. Graphs b) and d) show the same for the wave initially in the second mode. Entering the waveguide from the left the resulting wave intensity is almost entirely composed of the first mode, independently on the initial wave configuration. Entering the waveguide from the right the resulting wave intensity is mostly composed from the second mode. This behaviour confirms the successful asymmetric switching.

Eq. (S.50) reads

$$\Delta(x) = \frac{d(\delta(x)x)}{dx} = \pm\Delta_0(2x/L - 1) + \rho', \tag{S.63}$$

where $\Delta_0 = 2\delta_0$ and $\rho' = \delta_0 + \rho$ are the renormalized detuning and offset, respectively. As an example, the contours of the infinite waveguide corresponding to the finite waveguide defined by Eqs. (S.60) and (S.61) at the position $x_0 = 16W$ are shown as green curves in the upper panel of Fig. S5. As expected, in order to achieve successful RAP the renormalized detuning Δ defined in Eq.(S.63) is swept through the forward scattering resonance at $\Delta = 0$.

Then, the Hamiltonian describing the microwave transport in the finite waveguide can be written as

$$\mathcal{H} = \frac{1}{2}\begin{bmatrix} -\Delta & \Omega \\ \Omega & \Delta \end{bmatrix} - i\eta \begin{bmatrix} \Gamma_{11} & \Gamma_{12} \\ \Gamma_{12}^* & \Gamma_{22} \end{bmatrix}, \tag{S.64}$$

with $\Omega(x) = 2B\sigma(x)$. In the theoretical calculations and the experimental realization, we locate the absorber in the finite waveguide in the interval $7W < x < 18W$. To reduce the undesired backscattering, the strength (thickness) of the absorber smoothly fades in and out at both ends described by the function

$$\eta(x) = \begin{cases} \frac{\eta_0}{4}\left\{1 - \cos\left[\frac{2\pi(x-7W)}{11W}\right]\right\}^2, & 7W \leq x \leq 18W \\ 0, & \text{elsewhere.} \end{cases} \tag{S.65}$$

In our following semi-analytical calculations, the width of the absorber is $d = 0.019W$ and the absorption strength $\eta_0 W = 61$. Driven by the Hamiltonian from Eq. (S.64), the theoretically calculated evolution of the amplitudes c_1 (black lines) and c_2 (red lines) of the first and second propagation mode ($kW/\pi = 2.6$) along the waveguide is shown in Fig. S6 for the empty waveguide and Fig. S7 for the waveguide with absorber. Panels a) and c) depict the wave entering the waveguide in the first mode from the left and right, respectively. Graphs b) and d) show the same for the wave initially in the second mode. Arrows mark the direction of the wave propagation. Solid curves denote the results from numerical simulations based on the recursive Green's function method and the dotted curves correspond to the semi-analytical calculation based on the Schrödinger equation (S.49) with the Hamiltonian from Eq. (S.64).

In the Hermitian case [Fig. S6] the population of the modes almost perfectly flips during the propagation for both encircling directions, which demonstrates faithful RAP. In the non-Hermitian case [Fig. S7] the right propagating waves end up almost entirely in the first mode for arbitrary initial wave configurations. On the other hand, the left propagating waves end up almost entirely in the second mode. This clearly proves a successful asymmetric switching. Both figures confirm that the results of the semi-analytical model agree very well with the results of the numerical simulation.

The values of c_1 and c_2 shown here were used to calculate the population inversion p in Fig. 3(c–f) in the main text. The mode populations from our semi-analytical and numerical calculations shown in Fig. 3(c–f) in the main text nicely reproduce the behavior of the simple model driven by the Hamiltonian (S.9) with level populations shown Fig. 2 in the main text. The only significant difference is observed in Fig. 3(f) in the main text, where the state initially in the first mode (violet curve) evolves adiabatically instead of experiencing two non-adiabatic jumps as observed in Fig. 2(f) in the main text. This difference is caused by the fact that in contrast to the simple model the parameter evolution in the waveguide starts at the $\mathrm{Im}\lambda = 0$ line [black dashed line in Fig. S8(b), see next subsection] since there is no absorber present initially [3]. Chirality of the evolution is preserved, however, since zero or two non-adiabatic jumps both lead to the same final state.

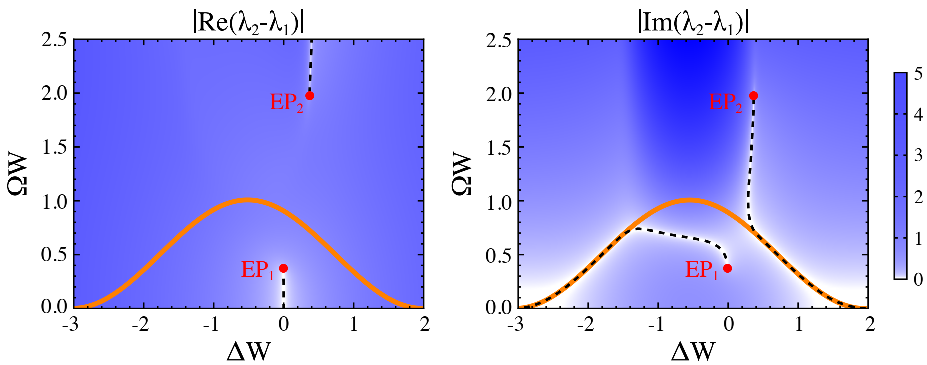

Figure S8: Difference of the real (left panel) and imaginary (right panel) parts of the eigenvalues of the extended non-Hermitian Hamiltonian [Eq. (S.66)]. Red dots mark the positions of the EPs and the black dashed lines correspond to $\mathrm{Re}\,\lambda_1 = \mathrm{Re}\,\lambda_2$ (left panel) and $\mathrm{Im}\,\lambda_1 = \mathrm{Im}\,\lambda_2 = 0$ (right panel). The orange curve denotes the parametric loop corresponding to the finite waveguide. The loop starts at the $\mathrm{Im}\,\lambda = 0$ line and encircles one of the EPs.

Position of the EP

The Hamiltonian in Eq. (S.64) that drives the microwave transport in a finite waveguide in the presence of a continuous position-dependent absorber is in principle defined only along the specific parametric loop given by Eqs. (S.60) and (S.63). Since successful RAP and asymmetric switching is closely related to the position of the DP and EP with respect to the parameter path, we have to extend the definition of the Hamiltonian [Eq. (S.64)] to the entire parameter plane (Δ, Ω) in order to locate those points. We choose the extended Hamiltonian in the form

$$\begin{aligned}\mathcal{H}(\Delta,\Omega) = \mathcal{H}_0(\Delta,\Omega) \\ + i\eta_0 k\Bigg\{\tilde{\eta}(\Delta)\left[1-f(\Delta,\Omega)\right]\left[\frac{\Omega}{\Omega_L(\Delta)}\right]^2\begin{bmatrix}\Gamma_{11} & \Gamma_{12}\\ \Gamma_{12}^* & \Gamma_{22}\end{bmatrix} \\ + \tilde{\eta}_{\mathrm{hom}}(\Delta)\frac{f(\Delta,\Omega)}{50}\begin{bmatrix}\frac{1}{k_1} & 0\\ 0 & \frac{1}{k_2}\end{bmatrix}\Bigg\},\end{aligned} \quad \text{(S.66)}$$

where

$$\mathcal{H}_0(\Delta,\Omega) = \frac{1}{2}\begin{bmatrix}\Delta & \Omega\\ \Omega & -\Delta\end{bmatrix}, \quad f(\Delta,\Omega) = \frac{\Omega_L^2(\Delta)-\Omega^2}{\Omega_L^2(\Delta)} \quad \text{(S.67)}$$

and

$$\Omega_L(\Delta) = B\sigma_0\left[1+\cos\left(\pi\frac{\Delta-\rho'}{\Delta_0}\right)\right]. \quad \text{(S.68)}$$

The non-Hermitian part of the extended Hamiltonian [Eq. (S.66)] is an interpolation between the losses due to the continuous thin absorber defined on the parametric loop and the homogeneous absorption for the straight waveguide. The strength of the position-dependent absorber located at $7W < x < 18W$ extended to the parameter plane reads

$$\tilde{\eta}(\Delta) = \begin{cases} \frac{1}{4}\left[1 - \cos\left(2\pi \frac{X(\Delta)-7W}{11W}\right)\right]^2, & 7W < X(\Delta) < 18W \\ 0, & \text{elsewhere} \end{cases} \tag{S.69}$$

with

$$X(\Delta) = \left(\frac{\Delta - \rho'}{\Delta_0} + 1\right)\frac{L}{2} \tag{S.70}$$

and the strength of the homogeneous absorption present in the whole waveguide is

$$\tilde{\eta}_{\mathrm{hom}}(\Delta) = \frac{1}{4}\left[1 + \cos\left(\pi \frac{\Delta - \rho'}{\Delta_0}\right)\right]^2. \tag{S.71}$$

The DP of the Hermitian part $\mathcal{H}_0$ is simply positioned at $(\Omega_{\mathrm{DP}} = 0, \Delta_{\mathrm{DP}} = 0)$ where the eigenvalues of $\mathcal{H}_0$ coalesce. The locations of the EPs of the non-Hermitian Hamiltonian have to be extracted numerically solving $\lambda_1 = \lambda_2$ where λ_j are the complex eigenvalues of $\mathcal{H}$. The real and imaginary parts of the eigenvalues λ of the extended non-Hermitian Hamiltonian [Eq. (S.66)] are shown in Fig. S8. The orange solid curve corresponds to the parameter loop and the red dots define the position of the EPs. Black dashed curves denote the lines where $\mathrm{Re}\,\lambda_1 = \mathrm{Re}\,\lambda_2$ (left panel) and $\mathrm{Im}\,\lambda_1 = \mathrm{Im}\,\lambda_2 = 0$ (right panel). As expected, the loop encircles one of the EPs. Moreover, since the absorber is not present at the very beginning and end of the waveguide the eigenvalues are entirely real ($\mathrm{Im}\,\lambda = 0$) for $x < 7$ and $x > 18$. Note that there is in principle the freedom to choose the extension of the Hamiltonian arbitrarily which in turn results in different positions for the EP. The only thing that has to be satisfied when the Hamiltonian is extended to the entire (Ω, Δ)-plane is that the additional Hamiltonian must coincide with the original Hamiltonian along the predefined parameter loop. In fact, the exact position of the EP inside the loop is not important. The crucial point is that the EP is encircled, which can be seen from the topology of the eigenvalues of the Hamiltonian following the parameter loop.

References

[1] V. S. Malinovsky and J. L. Krause, *Eur. Phys. J. D* **14**, 147 (2001).

[2] J. Doppler, A. A. Mailybaev, J. Böhm, U. Kuhl, A. Girschik, F. Libisch, T. J. Milburn, P. Rabl, N. Moiseyev, and S. Rotter, *Nature* **92**, 052124 (2016).

[3] T. J. Milburn, J. Doppler, C. A. Holmes, S. Portolan, S. Rotter, and P. Rabl, *Phys. Rev. A* **92**, 052124 (2015).